48th AIAA Aerospace Sciences Meeting Including the New Horizons Forum and Aerospace Exposition
4 - 7 January 2010, Orlando, Florida

AIAA 2010-838

Simulation of CAA Benchmark Problems Using High-Order Spectral Difference Method and Perfectly Matched Layers

Ying Zhou[1] and Z.J. Wang[2]

Department of Aerospace Engineering and CFD Center, Iowa State University, Ames, IA 50011

The high-order spectral difference (SD) method is used for the numerical simulation of several benchmark problems in computational aeroacoustics (CAA) to assess its effectiveness. A Perfectly Matched Layer (PML) absorbing boundary condition is implemented in the SD solver to minimize artificial wave reflections at computational boundaries. The performance of PML is tested and compared with the characteristic boundary condition. The numerical solution of Problem 1 "single airfoil response of impinging gust" in Category 3 and Problem 2 "trailing edge noise problem" in Category 4 of the Fourth Computational Aeroacoustics (CAA) Workshop on Benchmark Problems[1] are presented here.

I. Introduction

Computational Aeroacoustics (CAA) studies the aerodynamic acoustic wave generation and propagation using computational simulations. In the past two decades, considerable progresses in CAA have been made. As numerical methods and boundary condition techniques for CAA mature, the interest in investigating "real-world" problems grows. Several such problems have been set and worked on in the Fourth Computational Aeroacoustics (CAA) Workshop on Benchmark Problems[1].

The acoustic disturbance amplitudes are usually several orders of magnitude smaller than the mean flow disturbance. In order to capture the small magnitude acoustic disturbance and minimize numerical dispersion, an important requirement of CAA is high-order method. In the past years, high-order finite difference methods and overset grid methods which can handle complex geometries have been developed and used as the main simulation methods in CAA. In the last two decades, there have been intensive research efforts on high-order methods for unstructured grids[2-13]. High-order methods on unstructured grid are known for their advantages of robustness and reliability in numerical simulation of multiple-scale flow with complex geometries. A high-order SD method for the three dimensional Navier-Stokes equations on unstructured hexahedral grids developed by Sun et al.[13] is used for the numerical simulation of aeroacoustic problems in this paper.

Boundary condition is another critical component in the development of CAA algorithms. For aeroacoustic problems, the proper artificial computational boundaries are needed to avoid the reflection of the out-going waves which contaminants the physical flow field. Various numerical non-reflecting boundary conditions[14-17] based on the characteristics of the Euler equations have been developed to minimize the reflection of out-going waves. In recent years, several kinds of the disturbance-absorbing and buffer/sponge zone technique[18-23] have been developed. In the disturbance-absorbing and buffer/sponge zone type of methods, additional zones surrounding the physical domain are introduced so that in the added zones either the outgoing disturbances are attenuated and thus the reflections are minimized[21-23], or the mean flow is altered gradually to be supersonic[18-20]. Recently, Hu et al.[21] introduced a Perfectly Matched Layer technique for absorbing out-going disturbances in a finite difference method of solving Euler equations and Navier-Stokes equations. The equations for PML are designed such that the out-going waves are absorbed by the layer with no reflection (theoretically) and the flow field recovers to a proposed mean flow at the end of the PML region. In this paper, the PML technique is implemented in the SD method with unstructured grids and used as the absorbing boundary condition in the numerical simulation of the aeroacoustic problems.

In the numerical experiments, the case of the propagation of an isentropic vortex is presented to verify the effectiveness and performance of the PML approach for the SD method solving the nonlinear Euler equations. In Benchmark Problem 1, the unsteady aerodynamic and acoustic responses of symmetric and Joukowski airfoils to an impinging 2D vertical gust are predicted with the nonlinear Euler equations. The prediction and reduction of unsteady airfoil noise is one of the main issues for reducing overall acoustic emission for subsonic vehicles. In

---

[1] Ph.D. Candidate, Dept. of Aerospace Engineering, 0245 Howe Hall, ying@iastate.edu, AIAA student member.
[2] Professor of Aerospace Engineering, 2271 Howe Hall, zjw@iastate.edu, Associate Fellow of AIAA.

Benchmark Problem 2, the trailing edge noise problem solving Navier-Stokes equations is employed. For subsonic flow, one of the primary sources of trailing edge noise corresponds to the receptivity, excitation of the shear layer. The various mechanisms contributing to this problem include the interaction between acoustic waves, shear layer, and unsteady disturbances, which is a challenge to the numerical method and boundary conditions. All the results of these numerical experiments show that the high-order SD method with PML is capable of capturing the aeroacoustic disturbances.

The paper is organized as follows. In the next section, the formulation of the 3D SD method for a hexahedral element is reviewed. In Section 3, the formulation and implementation of the PML technique in the SD method is described. In Section 4, the numerical simulation results of the aeroacoustic problems are presented and discussed. Conclusions are summarized in Section 5.

II. Review of Multidomain Spectral Difference Method

We consider the unsteady three-dimensional compressible nonlinear Navier-Stokes equations written in the conservative form as

$$\frac{\partial Q}{\partial t} + \frac{\partial F}{\partial x} + \frac{\partial G}{\partial y} + \frac{\partial H}{\partial z} = 0 \tag{1}$$

on domain $\Omega \times [0, T]$ and $\Omega \subset R^3$ with the initial condition

$$Q(x, y, z, 0) = Q_0(x, y, z) \tag{2}$$

and appropriate boundary conditions on $\partial\Omega$. In (1), x, y, and z are the Cartesian coordinates and $(x, y, z) \in \Omega$, $t \in [0, T]$ denotes time, Q is the vector of conserved variables, and F, G and H are the fluxes in the x, y and z directions, respectively.

In SD method, it is assumed that the computational domain is divided into non-overlapping unstructured hexahedral cells or elements. In order to handle curved boundaries, both linear and quadratic isoparametric elements are employed, with linear elements used in the interior domain and quadratic elements used near high-order curved boundaries. In order to achieve an efficient implementation, all physical elements (x, y, z) are transformed into standard cubic element $(\xi, \eta, \varsigma) \in [0,1] \times [0,1] \times [0,1]$ as shown in Figure 1.

Physical element   Standard cubic element
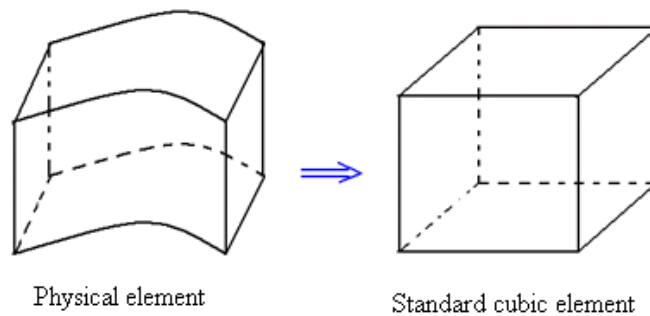
Figure 1: Transformation from a physical element to a standard element

In the standard element, two sets of points are defined, namely the solution points and the flux points. The solution unknowns or degrees-of-freedom (DOFs) are the conserved variables at the solution points, while fluxes are computed at the flux points in order to update the solution unknowns. At the interfaces between each two elements, a Riemann solver (Roe flux[24]) is used to compute the common inviscid flux, and the viscous flux at the interface is computed following the algorithm given in[25]. A detailed description of the space discretization and the algorithm in SD method to compute the inviscid flux and viscous flux derivatives can be found in [13].

III. Formulation of Perfectly Matched Layer

The Perfectly Matched Layer (PML) technique[21] is an absorbing boundary condition to truncate the physical domain, and is implemented in this paper for the high-order SD solver. The equations in the PML zone are formulated so that the amplitude of the out-going waves $Q' = Q - \bar{Q}$ entering the PML zone can be exponentially reduced while causing as little numerical reflection as possible. So a mean state of flow $\bar{Q}$ satisfies (3) is needed for the unsteady

flow variables Q to reduce to. The governing Equation (4) is obtained by subtracting the mean state Equations (3) from the original Navier-Stokes Equations (1).

$$\frac{\partial F(\overline{Q})}{\partial x} + \frac{\partial G(\overline{Q})}{\partial y} + \frac{\partial H(\overline{Q})}{\partial z} = 0 \tag{3}$$

$$\frac{\partial Q'}{\partial t} + \frac{\partial (F - F(\overline{Q}))}{\partial x} + \frac{\partial (G - G(\overline{Q}))}{\partial y} + \frac{\partial (H - H(\overline{Q}))}{\partial z} = 0 \tag{4}$$

A three-step transformation process to formulate the PML equations based on (4) is described in [21]:
1. **A proper space-time transformation**
2. **A PML change of variables in the frequency domain**
3. **A transformation from the frequency domain equation to the time domain equation**

The PML equations (5) - (14) are obtained by following the above steps. More detailed description of deriving PML equations can be found in [21].

$$\frac{\partial\left(Q - \overline{Q}\right)}{\partial t} + \frac{\partial\left(F - \overline{F}\right)}{\partial x} + \frac{\partial\left(G - \overline{G}\right)}{\partial y} + \frac{\partial\left(H - \overline{H}\right)}{\partial z} + \sigma_x q_1 + \sigma_y q_2 + \sigma_z q_3 + \beta\sigma_x\left(F - \overline{F}\right) = 0 \tag{5}$$

$$\frac{\partial q_1}{\partial t} + \frac{\partial\left(F - \overline{F}\right)}{\partial x} + \sigma_x q_1 + \beta\sigma_x\left(F - \overline{F}\right) = 0 \tag{6}$$

$$\frac{\partial q_2}{\partial t} + \frac{\partial\left(G - \overline{G}\right)}{\partial y} + \sigma_y q_2 = 0 \tag{7}$$

$$\frac{\partial q_3}{\partial t} + \frac{\partial\left(H - \overline{H}\right)}{\partial z} + \sigma_z q_3 = 0 \tag{8}$$

$$\frac{\partial r_1}{\partial t} + \sigma_x r_1 = \frac{\partial\left(G - \overline{G}\right)}{\partial x} + \beta\sigma_x\left(U - \overline{U}\right) \tag{9}$$

$$\frac{\partial r_2}{\partial t} + \sigma_y r_2 = 0 \tag{10}$$

$$\frac{\partial r_3}{\partial t} + \sigma_z r_3 = 0 \tag{11}$$

$$e_1 = \frac{\partial U}{\partial x} - \sigma_x r_1 + \beta\sigma_x\left(U - \overline{U}\right) \tag{12}$$

$$e_2 = \frac{\partial U}{\partial y} - \sigma_y r_2 \tag{13}$$

$$e_3 = \frac{\partial U}{\partial z} - \sigma_z r_3 \tag{14}$$

where $U = (u \ v \ w \ T)^T$ are the variables whose spatial derivative is present in the viscous flux vectors.

The PML Equations (5)-(14) are valid only in the PML region as shown in Figure 2. In [21], the PML absorption coefficient in x direction is taken to be

$$\sigma_x = \sigma_{max}\left|\frac{x - x_0}{D_x}\right|^\alpha \tag{15}$$

where σ_{max} and α are parameters that will be defined later, x_0 is the location of interface between the PML and physical domains and D_x is the width of the PML domain as shown in Figure 2. The absorption coefficients in the other two directions are defined in a similar way. And we use a simple empirical formula for β given in [22],

$$\beta = \frac{U_0}{1 - U_0^2}, \quad \text{where} \quad U_0 = \frac{1}{b - a}\int_b^a \overline{u}(y)dy \tag{16}$$

The computational domain for y direction is $[a, b]$ and $\overline{u}(y)$ is the mean velocity problem in x direction.
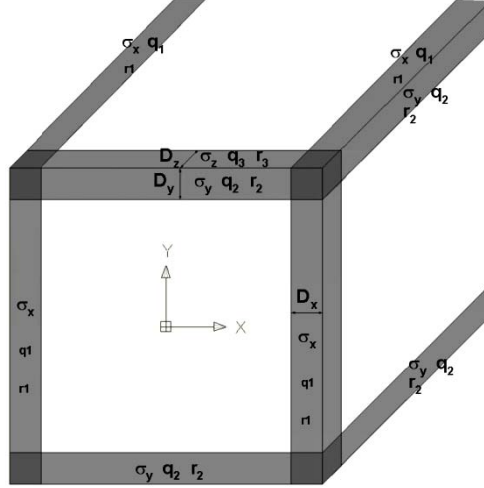
Figure 2: The schematics of the physical and PML domains (shadow). The sub-domains where the absorption coefficients are non-zero are indicated by arrows.

In all the numerical experiments of this paper, Cartesian coordinate grid is used in PML zone such that Equations (5)-(14) can be solved directly without the mesh transformation as in the usual SD method. The unknowns $\{Q, q_1, q_2, q_3, r_1, r_2, r_3\}$ are discretized in the same way as in SD method. As in Equations (5)-(14) the inviscid and viscous fluxes keep in the same forms as in Navier-Stokes equation (1), the common inviscid flux and viscous flux at the interfaces between each two element in PML zone are computed in the same manner as the usual SD method described in section 1.

IV. Numerical Experiments

Propagation of an Isentropic Vortex

To verify the effectiveness and performance of the PML approach for the SD method to solve the nonlinear Euler equations, the case of the propagation of an isentropic vortex is employed here. The two-dimensional nonlinear Euler equations support an advective solution of the form

$$
\begin{pmatrix} \rho \\ u \\ v \\ p \end{pmatrix} = \begin{pmatrix} 0 \\ U_0 \\ V_0 \\ 0 \end{pmatrix} + \begin{pmatrix} \rho' \\ u' \\ v' \\ p' \end{pmatrix}, \text{ where } \begin{cases} u' = -u_r \sin\theta \\ v' = u_r \cos\theta \\ \rho' = \left(1 - \frac{1}{2}(\gamma-1)U_{max}'^2 e^{1-\frac{r'^2}{r_0^2}}\right)^{1/(\gamma-1)} \\ p' = \frac{1}{\gamma}\left(1 - \frac{1}{2}(\gamma-1)U_{max}'^2 e^{1-\frac{r'^2}{r_0^2}}\right)^{1/(\gamma-1)} \end{cases}, \quad \begin{array}{l} r = \sqrt{(x - U_0 t)^2 + (y - V_0 t)^2}, \\ (U_0, V_0) = (0.5, 0.0), \\ U_{max} = 0.5 U_0 = 0.25, \\ \text{and } r_0 = 0.2 \end{array}
\tag{17}
$$

The Euler equations are solved with the 5th-order SD method in space and an explicit 3rd-order Runge-Kutta method[13] in time. The computation domain is $[-1.25, 1.25] \times [-1.25, 1.25]$, in which the PML domain is added around the physical domain of $[-1.0, 1.0] \times [-1.0, 1.0]$. The number of elements in the physical domain is 160 (resulting in 800 degrees-of-freedom), and in the PML domain 5 elements are added in each direction. In the PML domain, the parameters of absorption coefficient in (15) are set to be $\sigma_{max} = 20$ and $\alpha = 4$. In this case, the mean flow $\bar{Q}$ is,

$$
\begin{pmatrix} \bar{\rho} \\ \bar{U} \\ \bar{V} \\ \bar{p} \end{pmatrix} = \begin{pmatrix} 1.0 \\ 0.5 \\ 0.0 \\ 1/\gamma \end{pmatrix}
\tag{18}
$$

Figure 3 shows the v-velocity contours at time $t = 0.5, 1.5, 2.0$ and 3.0 respectively, at levels from ± 2.0 to ± 4.0. The absorption of the vortex in the PML domain is clearly demonstrated. In figure 4, the v-velocity profile along $y = 0$ at time $t = 0.5, 1.5, 2.0$ and 3.0 respectively is compared with the exact solution. It is shown that in the physical domain, the numerical solution matches the exact solution very well, while in the PML domain the solution decays exponentially and reduces to the mean state of flow near the end of PML domain.

Figure 5 shows the error of v-velocity with PML technique at time $t = 2.0$, and also the error of the same case with the characteristic boundary condition[17]. It is shown that the error of the numerical results with PML is indeed quite small and much smaller than that of the results with characteristic boundary condition. It is also noted that the error can be further decreased by increasing the width of the PML domain.

Benchmark CAA Problem 1

The numerical solution of the gust response problem for a symmetric Joukowski airfoil in a two-dimensional gust of Problem 1 in Category 3 of Fourth Computational Aeroacoustics Workshop on Benchmark Problems[1] is presented here. According to the formulation of the benchmark problem, the vertical gust harmonic is initially imposed on the mean flow with the following distribution:

$$u_{gust} = \frac{\varepsilon k_2}{\sqrt{k_1^2 + k_2^2}} \cos(k_1 x + k_2 y - \omega t)$$

$$v_{gust} = \frac{\varepsilon k_1}{\sqrt{k_1^2 + k_2^2}} \cos(k_1 x + k_2 y - \omega t)$$

(19)

where ε is the gust intensity relative to the mean flow, k_1 and k_2 are the gust wave numbers in the x and y directions, and ω is the imposed gust frequency. The mean flow $\bar{Q}$ is defined far upstream from the airfoil as:

$$\begin{pmatrix} \bar{\rho} \\ \bar{U} \\ \bar{V} \\ \bar{p} \end{pmatrix} = \begin{pmatrix} 1.0 \\ U \\ 0.0 \\ 1/\gamma \end{pmatrix}$$

(20)

where U is the upstream mean flow Mach number, and $\gamma = 1.4$. In all computations, the Mach number is fixed at $Ma = 0.5$, the gust intensity is $\varepsilon = 0.02$. Here we take $k_1 = k_2 = k$ and gust frequency is $\omega = kU$. The detailed problem description can be found in [1].

The 3rd-order SD method is used for space discretization and an explicit 3rd-order Runge-Kutta method is used for time integration. Figure 6 shows the computational mesh with the number of cells to be 39,550 which results in 355,950 degrees-of-freedom for the 3rd-order SD method. A PML zone with width $D = 10$ is added to the upper and outer boundary of the physical domain, and the interfaces between the PML zone and physical domain are shown by the dash line in Figure 6. The parameters of absorption coefficient in (15) are set to be $\sigma_{max} = 20$ and $\alpha = 4$ in this case.

The calculated mean pressure on the surface of the symmetric airfoil is shown in Figure 7, in comparison with the result in [1]. Figure 8 shows the calculated root mean square (RMS) of the pressure on the upper and lower surfaces of the airfoil respectively for wave number $k = 1.0$ and $k = 2.0$. Both the mean pressure and RMS pressure on the airfoil surface agree well with the results in [1]. Figure 9 shows the instantaneous velocity (y-component) contour field for wave number $k = 1.0$ and $k = 2.0$. Figure 10 shows the instantaneous velocity (y-component) profile along $x = 1$. Both Figure 9 and Figure 10 illustrate that the PML performs well in absorbing the out-going wave entering the PML zone and the flow variables Q reduce to the proposed mean flow $\bar{Q}$ at the end of the PML zone. The present results illustrate that the present numerical method and absorbing boundary condition are capable for numerical simulation of the gust-airfoil interaction problem using the non-linear Euler equations.

Benchmark CAA Problem 2

The numerical solution of the trailing edge noise problem of Problem 2 in Category 4 of Fourth Computational Aeroacoustics Workshop on Benchmark Problems[1] is presented here. Consider a two-dimensional, compressible mixing layer flow formed by a splitter plate with a blunt trailing edge, Figure 11. The splitter plate has a shape

consisting of a flat plate section capped by a super-ellipse at the trailing edge, and the definition of the splitter plate surface is:

$$\begin{cases} (y)^2 + \left(1 + \dfrac{x}{2.5}\right)^6 = 1, & -2.5 \le x \le 0 \\ y = \pm 1, & x < -2.5 \end{cases} \tag{21}$$

Figure 11 shows the computational grid with 8,000 element cells. The physical domain is $-30.0 \le x \le 100.0$, $-80.0 \le y \le 80.0$, and the PML domain is added around the physical domain with the width $D_{x-upstream} = 20$, $D_{x-downstream} = 50$ and $D_y = 20$ (Figure 11). And the parameters of absorption coefficient in (15) are set to be $\sigma_{max} = 40$ and $\alpha = 3$ in this case. Both the 3rd-order and 4th-order SD methods are used for space discretization; thus resulting in 72,000 and 128,000 degrees-of-freedom, respectively.

The upper and lower stream has free stream Mach number $Ma_1 = 0.1$ and $Ma_2 = 0.6$ respectively with the same boundary layer momentum thickness $\theta = 1.0$ at $x = -50$. The flow state at the inflow boundary at $x = -50$ is approximated above and below the plate by solutions to the compressible boundary layer equations with zero pressure gradients. Free stream conditions above the plate are $T_1 = T_2$ and $\rho_1 = \rho_2$. The Reynolds number based on the lower free stream properties and boundary layer momentum thickness is $Re = 250$. Boundary conditions on the plate surface are the non-slip condition $u = v = 0$ and the isothermal condition $T_{wall} = T_1$. More details of the description of this problem can be found in the Fourth Computational Aeroacoustics (CAA) Workshop on Benchmark Problems[1].

Steady State Solution
The mixing layer in the present case is strongly unstable and supports exponentially growing small disturbances. Using the traditional characteristic outlet boundary condition, the steady state is never achieved with a high-order method. The feedback from the outlet boundary reflection error must be less than the gain of the unstable shear layer, such that the flow could ultimately relax to a steady solution. In this paper, a steady solution was achieved with a relatively small PML sponge zone.

The mean flow $\bar{Q}$ for PML in Equation (3) is provided by the 1st-order steady solution with the characteristic outlet boundary condition. But the 1st-order mean flow $\bar{Q}$ does not exactly satisfy Equation (3) with higher order methods, so the mean flow $\bar{Q}$ is updated with an improved mean flow as the computation proceeds. With the PML and an improving mean flow, the computation converged and the L2 norm of the residues eventually becomes less than 10^{-8}, which is at least six orders of magnitude from its initial value.

Figure 12 shows the streamwise velocity profiles at $x = 75$ for the steady state solution. Results for the 3rd-order method and 4th-order method are indistinguishable from each other. Figure 13 shows the steady state streamwise velocity profile at $x = 5$, $x = 40$ and $x = 75$ and compares with the results of Barone et al.[1] at $x = 5$. Good agreement is found. The present results and comparison suggest that spatial convergence of the mean velocity profiles was obtained.

Evolution of a Pressure Pulse
This problem is to solve the scattering of an acoustic pulse which originates near the trailing edge. It involves a complicated physical process including the pressure pulse expanding and interacting with the trailing edge, and then the exciting and thereafter exponential growth of the Kelvin-Helmholtz instability wave packet within the shear layer. To capture the reflected component, the transmitted component, and the diffracted component of the scattering pressure pulse, the 4th-order SD method and an explicit 3rd-order Runge-Kutta method are used for the spatial discretization and time integration respectively. The initial condition of this initial value problem of a pressure pulse superimposed on the steady flow is

$$U(x, y, 0) = \bar{U}(x, y) + \begin{bmatrix} 0 \\ 0 \\ 0 \\ f(x, y) \end{bmatrix}, \qquad \text{where } \bar{U}(x, y) \text{ is the steady solution and} \qquad f(x, y) = \frac{0.05}{\gamma - 1} e^{-\ln 2 \left[\left(\frac{x+20}{4} \right)^2 + \left(\frac{y+20}{4} \right)^2 \right]}, \; \gamma = 1.4 \tag{22}$$

Figure 14 shows the computed pressure disturbance distribution of the 4th-order solution within the shear layer at $y = -3$ for $t = 200$. The dash lines represent interfaces between the physical domain and PML zones, and the absorbing processes are clearly shown in both upstream PML zone $-50 \le x \le -30$ and downstream PML zone

$100 \leq x \leq 150$. Figure 15 gives the acoustic signal recorded at $(x, y) = (-30, 1)$ for the time duration $40 \leq t \leq 80$. Both results of the pressure disturbance distribution (Figure 14) and the acoustic signal serial (Figure 15) are compared with the results of Barone et al.[1]. Good agreements are found and the physics are seen to be well captured by the 4th-order SD method and the 3rd-order Runge-Kutta method.

V. Conclusions

In this paper, a time-domain absorbing boundary condition PML for nonlinear Euler and Navier-Stokes equations has been implemented for the high-order SD method with unstructured grids. In the numerical verification case of the isentropic vortex propagation, it is shown that the error of the numerical results with PML is about two orders lower than that of the results with characteristic boundary condition. Two benchmark problems in the Fourth Computational Aeroacoustics (CAA) Workshop on Benchmark Problems have been tested. The results show that the high-order SD method with unstructured grid is capable for the numerical simulation of aeroacoustic problems and the performance and efficiency of the PML are good in these cases.

Acknowledgements

References

[1] Fourth Computational Aeroacoustics (CAA) Workshop on Benchmark Problems, NASA/CP—2004-212954

[2] Patera, A.T., A Spectral element method for fluid dynamics: Laminar flow in a channel expansion, J. Comput. Phys. 54, 468(1984).

[3] Kopriva, D.A. and Kolias, J.H., A conservative staggered –grid Chebyshev multidomain method for compressible flows, J. Comput. Phys. 125, 244(1996).

[4] Barth, T.J. and Frederickson, P.O., High-Order Solution of the Euler Equations on Unstructured Grids using Quadratic Reconstruction, AIAA Paper No. 90-0013(1990).

[5] Hu, C. and Shu, C.-W., Weighted essentially non-oscillatory schemes on triangular meshes, J. Comput. Phys. 150, 97 (1999).

[6] Cockburn, B. and Shu, C.-W., TVB Runge-Kutta local projection discontinuous Galerkin finite element method for conservation laws II: General framework, Math. Comput. 52,411(1989).

[7] Abgrall, R. and Roe, P.L., High Order Fluctuation Schemes on Triangular Meshes, Journal of Scientific Computing, Volume 19, pp. 3 – 36, 2003.

[8] Wang, Z.J. and Liu, Yen, Spectral (Finite) Volume Method for Conservation Laws on Unstructured Grids III: Extension to One-Dimensional Systems, J. Scientific Computing, Vol. 20 No. 1, pp.137-157 (2004).

[9] Liu, Y., Vinokur, M., and Wang, Z.J., Discontinuous Spectral Difference Method for Conservation Laws on Unstructured Grids, in Proceeding of the 3rd International Conference in CFD, Toronto, Canada July 2004.

[10] Liu, Yen, Vinokur, M., and Wang, Z.J., Multi-Dimensional Spectral Difference Method for Unstructured Grids, AIAA-2005-0320.

[11] Wang, Z. J., and Liu, Yen, The Spectral Difference Method for the 2D Euler Equations on Unstructured Grids, AIAA-2005-5112.

[12] Huang, P.G., Wang, Z.J., and Liu, Yen, An Implicit Space-Time Spectral Difference Method for Discontinuity Capturing Using Adaptive Polynomials,   AIAA-2005-5255.

[13] Y. Sun, Z.J. Wang, Y. Liu, High-Order Multidomain Spectral Difference Method for the Navier-Stokes Equations on Unstructured Hexahedral Grids, Communications in Computational Physics, Vol. 2, No. 2(2007) 310-333.

[14] K. W. Thompson, Time-dependent boundary conditions for hyperbolic systems, J. Comput. Phys., 68, 1-24(1987).

[15] M. B. Giles, Non-reflecting boundary conditions for Euler equation calculations, AIAA J., 28, 2050-2058(1990).

[16] T. Poinsot, and S. K. Lele, Boundary conditions for direct simulation of compressible viscous flows, J. Comput. Phys., 101, 104-129(1992)

[17] C. Hirsch, Numerical Computation Of Internal And External Flows: Fundamentals Of Computational Fluid Dynamics, (2007)

[18] J. B. Freund, Proposed inflow/outflow boundary condition for direct computation of aerodynamic sound, AIAA J., 35(4), 740-742(1997).

[19] S. Ta'asan, and D. M. Nark, An absorbing buffer zone technique for acoustic wave propagation, AIAA J. 95-0164 (1995).

[20] C. L. Streett, and M. G. Macaraeg, Spectral multi-domain for large-scale fluid dynamics simulations, Int. J. Appl. Numer. Math., 6, 123-139 (1990)

[21] F. Q. Hu, X. D. Li and D. K. Lin, Absorbing boundary conditions for nonlinear Euler and Navier-Stokes equations based on the Perfectly Matched Layer technique , J. Comput. Phys., 227 4398-4424 (2008).

[22] F. Q. Hu, X.D. Li and D. K. Lin, PML absorbing boundary condition for non-linear aeroacoustics problems , AIAA paper 2006-2521, 2006

[23] F. Q. Hu, A Perfectly Matched Layer Absorbing Boundary Condition for Linearized Euler Equations With a Non-uniform Mean Flow , Journal of Computational Physics, Vol. 208, 469-492, 2005

[24] P. L. Roe, Approximate Riemann solvers, parameter vectors, and difference schemes, J. Comput. Phys. 43 (1981) 357-372.

[25] D.A. Kopriva, J.H. Kolias, A Staggered-Grid Multidomain Spectral Mthod for the Compressible Navier-Stokes Equations,J. Comput. Phys. 143 (1998) 125-158.
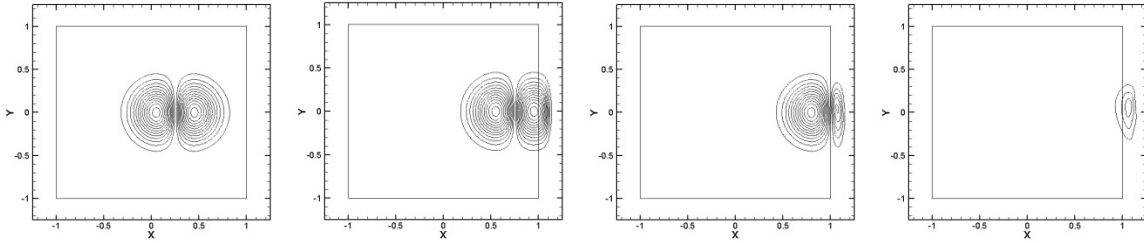
Figure 3: v-velocity contour levels at time (a) t=0.5, (b) t=1.5, (c) t=2.0 and (d) t=3.0 (from left to right). The solid square indicates the physical/PML interface
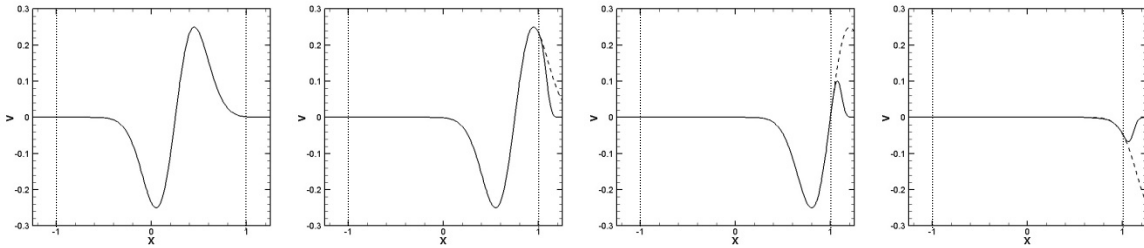
Figure 4: v-velocity profile along y=0 at time (a) t=0.5, (b) t=1.5, (c) t=2.0 and (d) t=3.0 (from left to right). Solid line: numerical solution; dashed line: exact solution
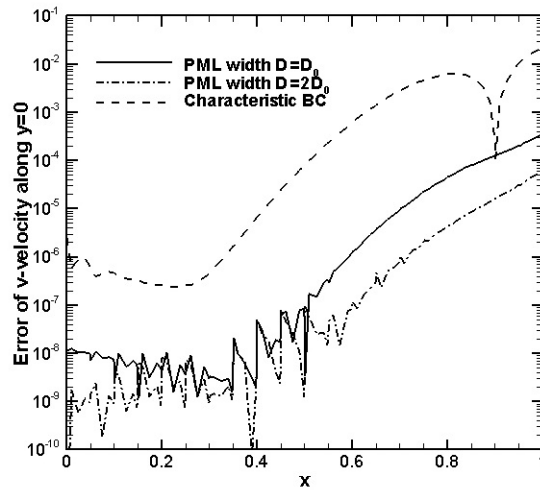
Figure 5: The error of v-velocity at time t = 2.0

American Institute of Aeronautics and Astronautics
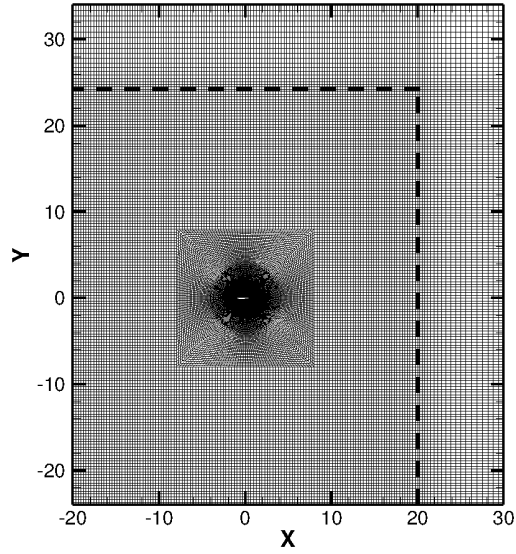
Figure 6 Computational mesh of Benchmark Problem 1
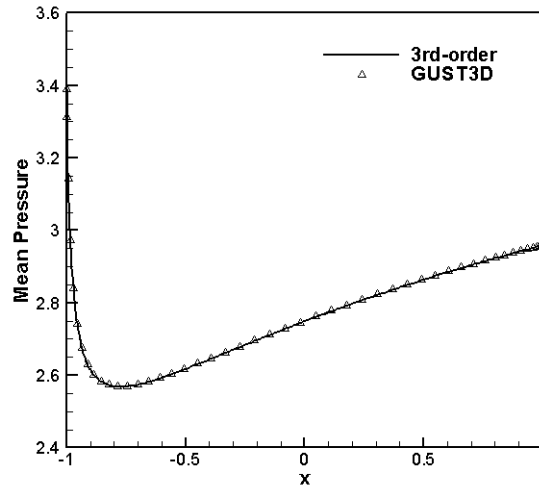
Figure 7: Mean airfoil surface pressure for the symmetric airfoil
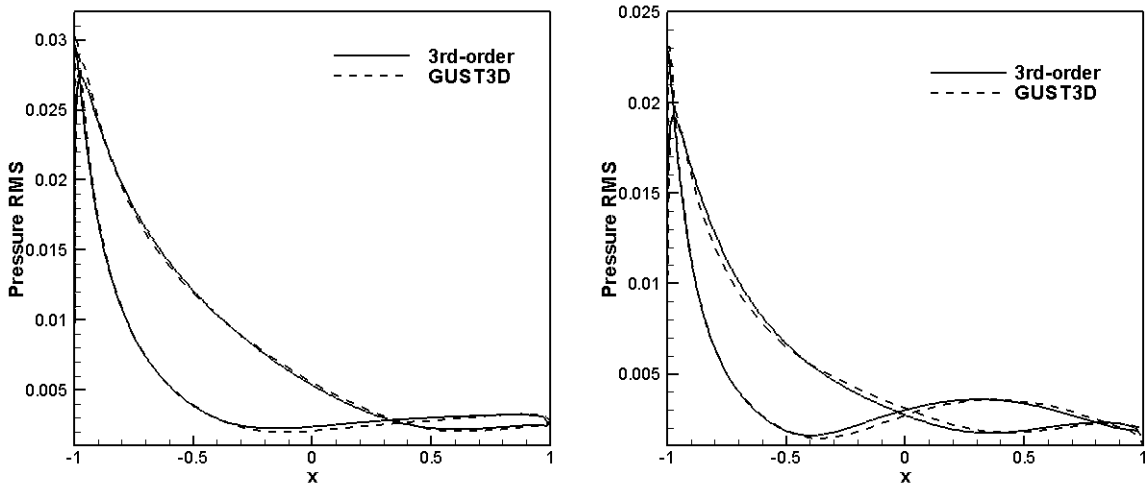
Figure 8: RMS pressure on the airfoil surface at wave number $k = 1.0$ (left) and $k = 2.0$ (right)

American Institute of Aeronautics and Astronautics
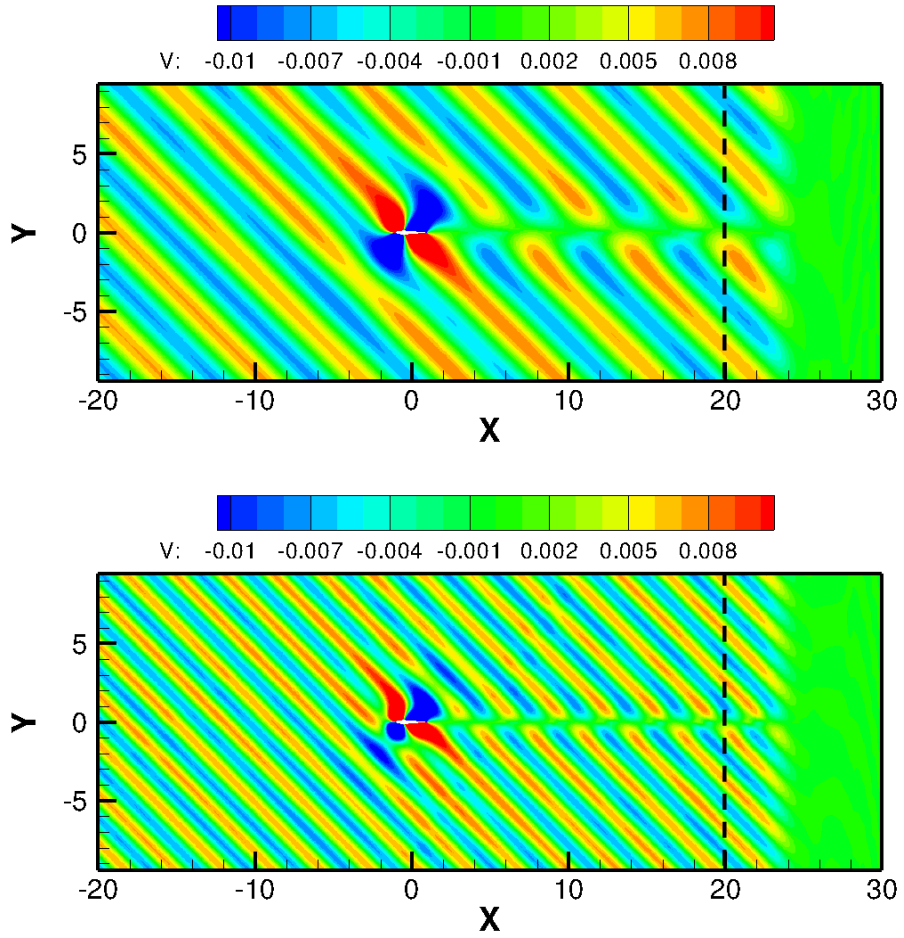
Figure 9: Instantaneous velocity contour, Y-component at wave number $k = 1.0$(upper) and $k = 2.0$(below)
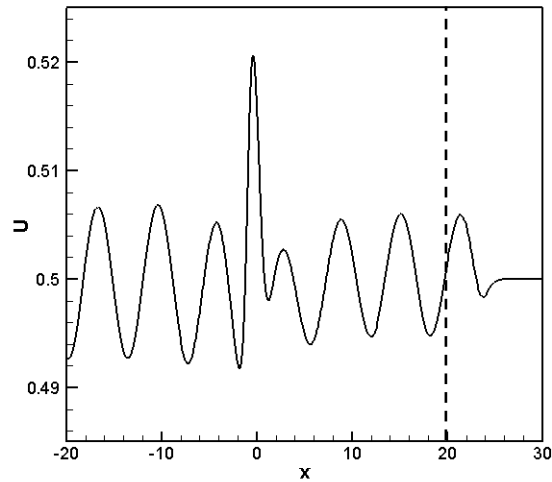
Figure 10: Instantaneous velocity profile along y = 1 at wave number $k = 1.0$
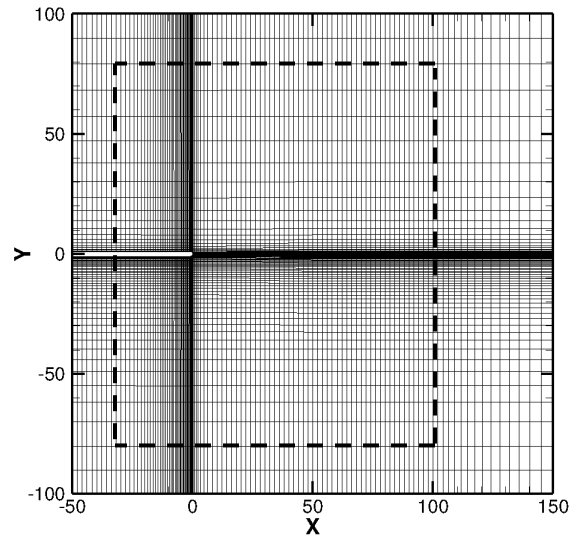
Figure 11 Computational mesh of Benchmark Problem 2
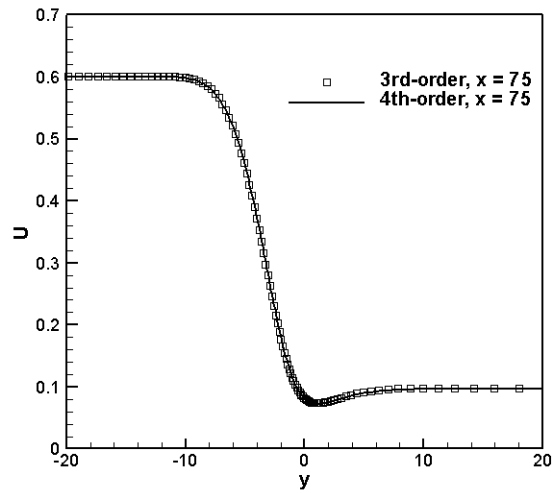
Figure 12 Steady state streamwise velocity profiles at $x = 75$
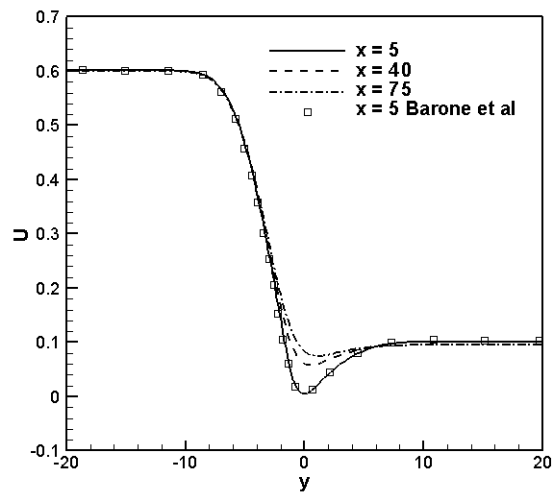
Figure 13 Steady state streamwise velocity profiles at $x = 5,$ $x = 40$ **and** $x = 75$
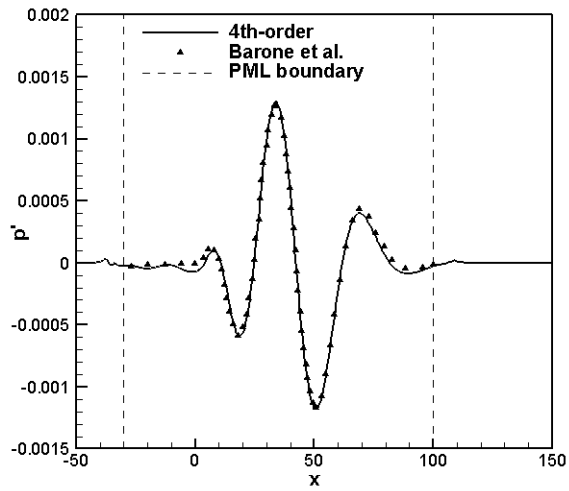
Figure 14 Pressure disturbances along the along $y = -3$ at $t = 200$
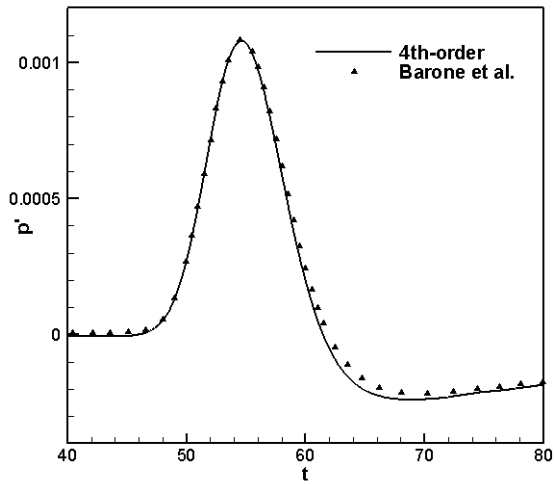
Figure 15 Acoustic pulse signals at $(x, y) = (-30, 1)$